An Extended Kalman Filter Based Automatic Frequency Control Loop

S. Hinedi
Communications Systems Research Section

A novel Automatic Frequency Control (AFC) loop based on an Extended Kalman Filter (EKF) is introduced and analyzed in detail. The new scheme involves an EKF which operates on a modified set of data in order to track the frequency of the incoming signal. The algorithm can also be viewed as a modification to the well known cross-product AFC loop. A low carrier-to-noise ratio (CNR), high-dynamic environment is used to test the algorithm and the probability of loss-of-lock is assessed via computer simulations. The scheme is best suited for scenarios in which the frequency error variance can be compromised to achieve a very low operating CNR threshold. This technique can easily be incorporated in the Advanced Receiver (ARX), requiring minimum software modifications.

I. Introduction

The algorithm introduced and analyzed herein is another application of the theory of Kalman filters [1] to the problem of estimating the parameters of a sinusoid embedded in noise. The use of Kalman filters in tracking time-varying parameters in general and the phase and/or the frequency of a sinusoidal signal in particular, has been well investigated by many researchers and is extensively documented in the literature [2]-[4]. In this particular application, the parameter of primary interest is the frequency of a pure sine wave which should be estimated in the presence of high dynamics at a low carrier-to-noise ratio (CNR). Typically, it is applied in a region where the Phase Locked Loop (PLL) loses lock frequently due to cycle slipping [5] and hence is unreliable.

The scheme sought should be easy to implement and possess the same order of complexity as the PLL. The goal here is to be able to track the frequency at a low CNR with a simple scheme that trades complexity for root-mean-squared (rms) frequency error performance. The automatic frequency control (AFC) algorithms discussed in the literature are typically more complex than the PLL [6], [7] except for the cross-product AFC loop, which performs poorly in terms of lowest operating CNR. In a typical operating environment, if the PLL loses lock due to a severe maneuver by the transmitter, the proposed simple AFC algorithm could then be used to track the doppler until the dynamics are well within the tracking capability of the PLL, which can then track again with the frequency initialization provided by the AFC algorithm.

II. Description and Analysis of Algorithm

One approach to tracking the frequency of a sinusoidal signal at a lower CNR than the PLL lies in modeling the dynamic process in differential form and hence tracking only the differential dynamics. Thus in this model, the phase process can not be tracked directly and is really compromised in order to further lower the threshold at which the frequency process can be estimated. However, given its initial value, the phase can later be derived from the frequency by integration, assuming the latter is estimated with a suitably small rms error.

There are numerous ways to arrive at a differential signal model to track the frequency; for example, each of the in-phase and quadrature samples at a specific time can be expanded using a Taylor series as a linear combination of the two previous samples [8] and that, after some further processing, can lead to a signal model in the desired form. The disadvantage of this scheme is that it tends to be quite computationally demanding because it considers higher-order approximations to the measurement function. In this article, the phase information is removed by manipulating the samples in a more direct manner, i.e., a simple cross-product between the in-phase and quadrature samples is performed in a manner similar to the cross-product AFC loop. The modified samples are then fed into an Extended Kalman Filter (EKF) that tracks the differential phase change from which the doppler can be deduced.

In the derivation to follow, the vector notation which is standard in the theory of Kalman filters is adopted. The received signal is observed in the presence of additive narrowband white gaussian noise with one-sided power spectral density N_0 (watts/Hz). The carrier is first removed by mixing the observed waveform with a fixed reference, after which the in-phase and quadrature signals are sampled at a fixed rate $f_s = T_s^{-1}$ where T_s is the sampling time. Hence the samples that need to be processed can be expressed in vector form as

$$\underline{r}(k) \triangleq \begin{bmatrix} r_I(k) \\ r_Q(k) \end{bmatrix} = \begin{bmatrix} A \sin\theta(k) \\ A \cos\theta(k) \end{bmatrix} + \underline{n}(k) \qquad (1)$$

where k is the discrete time, $\theta(k)$ the phase of the received signal, A its amplitude and $\underline{n}^T(k) = [n_I(k) \;\; n_Q(k)]$ is a zero mean gaussian vector, the subscripts I and Q denoting the in-phase and quadrature components respectively. Hence,

$$E[\underline{n}(k)] = \underline{0}$$

$$E[\underline{n}(k)\underline{n}^T(k)] = \left(\frac{N_0}{2T_s}\right)\underline{\underline{I}} \qquad (2)$$

where $\underline{\underline{I}}$ denotes the 2×2 identity matrix. Typically, the received samples $r_I(k)$, $r_Q(k)$ form the input to an EKF with a state vector consisting of the phase $\theta(k)$ and its various derivatives since the latter is modeled as a polynomial in time of sufficient degree to account for the dynamics encountered. The advantage of this approach is that it tracks the phase and frequency with small rms error when operating above threshold, defined here as the CNR at which frequency loss-of-lock occurs with a probability of 0.1. Because frequency is the primary parameter in this application, we expect to further lower the operating threshold by compromising the phase estimates and the rms error performance. The block diagram of the new scheme, referred to as Frequency EKF (FEKF), is shown in Fig. 1. The cross-product is performed in order to remove the phase from the samples, as follows

$$\begin{aligned} z_I(k) &= r_I(k)\,r_Q(k-1) - r_Q(k)\,r_I(k-1) \\ z_Q(k) &= r_I(k)\,r_I(k-1) + r_Q(k)\,r_Q(k-1) \end{aligned} \qquad (3)$$

In doing so, the effective noise has been increased and this will of course result in a larger frequency error. The modified samples $z_I(k)$ and $z_Q(k)$ are then used in the EKF which tracks only the differential phase, not the pseudo-phase. This results in a reduction in the order of the EKF and hence in complexity. Defining CNR as the carrier power to the one-sided power spectral density level of the noise, we have

$$CNR = \frac{A^2}{N_0} \qquad (4)$$

From Eq. (2), N_0 is equal to $2T_s\sigma^2$ where σ^2 is the variance of the noise samples $n_I(k)$, $n_Q(k)$. Hence, CNR can be expressed in terms of σ^2 as

$$CNR = \frac{A^2}{2T_s\sigma^2} \qquad (5)$$

Without loss in generality, we can now set A to unity, as the CNR and the sampled noise variance are inversely related by Eq. (5). Plugging Eq. (1) into Eq. (3) and expanding, we easily obtain

$$\begin{aligned} z_I(k) &= \sin\Delta\theta(k) + n_I'(k) \\ z_Q(k) &= \cos\Delta\theta(k) + n_Q'(k) \end{aligned} \qquad (6)$$

where the effective noises $n_I'(k), n_Q'(k)$ are given by

$$\begin{aligned} n_I'(k) &= n_I(k-1)\sin\theta(k) + n_Q(k)\cos\theta(k-1) \\ &\quad + n_I(k-1)n_Q(k) - n_Q(k-1)\cos\theta(k) \\ &\quad - n_I(k)\sin\theta(k-1) - n_I(k)n_Q(k-1) \\ n_Q'(k) &= n_Q(k-1)\sin\theta(k) + n_Q(k)\sin\theta(k-1) \\ &\quad + n_Q(k)n_Q(k-1) + n_Q(k-1)\cos\theta(k) \\ &\quad + n_I(k)\cos\theta(k-1) + n_I(k)n_I(k-1) \end{aligned} \tag{7}$$

and the differential phase at time k is defined by

$$\Delta\theta(k) = \theta(k) - \theta(k-1) \tag{8}$$

The differential phase itself can be modeled as an nth order polynomial whose derivatives constitute the components of the state vector $\underline{x}(k)$ of the FEKF as follows

$$\begin{aligned} \Delta\theta(k) &= \underline{\ell}^T \underline{x}(k) \quad ; \quad \underline{\ell}^T = [1, 0, \ldots, 0] \\ \underline{x}(k+1) &= \underline{\underline{\Phi}}\,\underline{x}(k) + \underline{v}(k) \end{aligned} \tag{9}$$

where $\underline{v}(k)$ is a disturbance term that models the random changes in parameters due to dynamics, and $\underline{\underline{\Phi}}$ denotes the state transition matrix. In the remainder of the paper, we will concentrate on the second-order FEKF, but the analysis can be generalized to any order. For a second-order FEKF, the state $\underline{x}^T(k)$ becomes

$$\underline{x}^T(k) = \left[\Delta\theta(k) \qquad \Delta\omega(k)\right] \tag{10}$$

where $\Delta\omega(k)$ is the derivative of $\Delta\theta(k)$. In that case, Eq. (9) yields

$$\begin{aligned} \Delta\theta(k+1) &= \Delta\theta(k) + T_s\Delta\theta(k) + v_1(k) \\ \Delta\omega(k+1) &= \Delta\omega(k) + v_2(k) \end{aligned} \tag{11}$$

where

$$v_i(k) = \int_{(k-1)T_s}^{kT_s} \frac{\tau^{2-i}}{(2-i)!} J(\tau)\, d\tau \quad ; \quad i = 1, 2 \tag{12}$$

In the above, $J(t)$ stands for jerk and denotes the second derivative of the differential phase or the third derivative of the pseudo-phase. Assuming that the jerk is a zero-mean white process with one-sided spectral level N_J, we obtain

$$E[v_2^2(k)] = \frac{N_J}{2} T_s = \sigma_J^2 T_s^2 \tag{13}$$

where σ_J^2 denotes the variance of the sampled version of $J(t)$. Denoting by $\underline{\underline{Q}}$ the covariance matrix of $\underline{v}(k)$, it is easily shown [3] that

$$\underline{\underline{Q}} = \sigma_J^2 T_s^2 \begin{bmatrix} \frac{T_s^2}{3} & \frac{T_s}{2} \\ \frac{T_s}{2} & 1 \end{bmatrix} \qquad \underline{\underline{\Phi}} = \begin{bmatrix} 1 & T_s \\ 0 & 1 \end{bmatrix} \tag{14}$$

The EKF equations are derived in [1] and are repeated below for convenience in recursive form.

$$\hat{\underline{x}}(k+1/k) = \underline{\underline{\Phi}}\;\hat{\underline{x}}(k/k-1) + \underline{\underline{K}}(k)\left[\underline{z}(k) - \underline{h}(\hat{\underline{x}}(k/k-1))\right] \tag{15a}$$

$$\underline{\underline{K}}(k) = \underline{\underline{\Phi}} \sum\!\!\!\!\sum (k/k-1)\underline{\underline{H}}(k)\left(\underline{\underline{H}}^T(k)\sum\!\!\!\!\sum (k/k-1)\underline{\underline{H}}(k) + \underline{\underline{R}}\right)^{-1} \tag{15b}$$

$$\begin{aligned} \sum\!\!\!\!\sum (k+1/k) &= \alpha^2 \underline{\underline{\Phi}}\left[\sum\!\!\!\!\sum (k/k-1) - \sum\!\!\!\!\sum (k/k-1)\underline{\underline{H}}(k)\right. \\ &\quad \cdot \left(\underline{\underline{H}}^T(k)\sum\!\!\!\!\sum (k/k-1)\underline{\underline{H}}(k) + \underline{\underline{R}}\right)^{-1} \\ &\quad \left. \cdot \underline{\underline{H}}^T(k)\sum\!\!\!\!\sum (k/k-1)\right]\underline{\underline{\Phi}}^T + \underline{\underline{Q}} \end{aligned} \tag{15c}$$

where

$$\underline{h}(\underline{x}(k)) = \begin{bmatrix} \sin(\underline{\ell}^T \underline{x}(k)) \\ \cos(\underline{\ell}^T \underline{x}(k)) \end{bmatrix}$$

$$\underline{\underline{H}}^T(k) = \frac{\partial}{\partial \underline{x}} \underline{h}(\underline{x})\Big|_{\underline{x}=\hat{\underline{x}}(k/k-1)} = \begin{bmatrix} \cos\Delta\hat{\theta}(k/k-1) & 0 \\ -\sin\Delta\hat{\theta}(k/k-1) & 0 \end{bmatrix} \tag{16}$$

and $\underline{\underline{R}}$ is the covariance matrix of the noise vector $\underline{n}'(k)$ given by

$$\underline{\underline{R}} = \sigma_n^2 \underline{\underline{I}} \quad ; \quad \sigma_n^2 = 2(\sigma^2 + \sigma^4) \tag{17}$$

The weighting coefficient α is typically used to adjust the classical trade-off between adaptation time in transient situations and steady-state error. The noise sequences $n_I'(k)$, $n_Q'(k)$ are colored but Eq. (17) reflects the statistics only at a specific time. No attempt is taken to whiten the sequences in order to abide with the original goal of a simple scheme. The weighting coefficient α can be used in addition to σ_J^2 to control the effective bandwidth of the EKF, as will be shown later in the linear analysis.

The performance of the FEKF operating in the presence of noise can only be derived in the steady-state, in which case the matrix $\underline{\underline{\Sigma}}(k+1/k)$ is independent of k. From Eq. (15c), it is not clear that the FEKF will reach steady state because $\underline{\underline{\Sigma}}(k+1/k)$ depends on the matrix $\underline{\underline{H}}(k)$ which in turn depends on the predicted value $\Delta\hat{\theta}(k/k-1)$. However, it is shown in the Appendix that the right-hand side of Eq. (15c) is in fact independent of $\Delta\hat{\theta}(k/k-1)$, and that both the linear and nonlinear filters reach the identical steady state. Furthermore, an equivalent steady-state nonlinear model is derived in the Appendix which is used to compute the error variance in white noise. Defining the steady-state matrix $\overline{\Sigma}$ to be

$$\overline{\Sigma} = \lim_{k\to\infty} \underline{\underline{\Sigma}}(k+1/k) \triangleq \begin{bmatrix} \sigma_1^2 & \rho \\ \rho & \sigma_2^2 \end{bmatrix} \tag{18}$$

the equivalent linear loop model is shown in Fig. 2 where $n_{eq}(k)$ denotes the equivalent noise given by

$$n_{eq}(k) = n_I'(k)\cos\Delta\hat{\theta}(k) - n_Q'(k)\sin\Delta\hat{\theta}(k) \tag{19a}$$

with power spectrum (assuming $\phi(k) = 0$)

$$S_{n_{eq}}(z) \triangleq -\sigma^2 z + 2(\sigma^2 + \sigma^4) - \sigma^2 z^{-1} \tag{19b}$$

Letting $\phi(k) \triangleq \Delta\theta(k) - \Delta\hat{\theta}(k)$ denote the differential error phase at time k, it is shown in the Appendix that the error variance is given by

$$\sigma_\phi^2 = T_s \int_{-\frac{1}{2T_s}}^{\frac{1}{2T_s}} \left| H\left(e^{js\pi fT_s}\right)\right|^2 S_{n_{eq}}\left(e^{j2\pi fT_s}\right) df \tag{20}$$

where $H(z)$ denotes the closed loop transfer function, related to the loop filter $F(z)$ via

$$H(z) \triangleq \frac{F(z)}{1+F(z)} = \frac{z(\sigma_1^2 + T_s\rho) - \sigma_1^2}{z^2(\sigma_1^2 + \sigma_n^2) + z(T_s\rho - \sigma_1^2 - 2\sigma_n^2) + \sigma_n^2} \tag{21}$$

The closed loop transfer function is depicted in Fig. 3 for a fixed α (1.005), N_J (200), and T_s(2 msec). The corresponding loop bandwidth B_L defined in the Appendix is shown in Fig. 4 versus the ratio σ_J^2/σ_n^2. When the measurement noise is dominant (i.e., $\sigma_J^2/\sigma_n^2 \ll 1$), the bandwidth is independent of CNR and is controlled by α. On the other hand, when the loop is dominated by the process noise (i.e., $\sigma_J^2/\sigma_n^2 \gg 1$), the bandwidth is a function of both CNR and α. The performance in the absence of dynamics is shown in Fig. 5 as a function of CNR when T_s = 2 msec. The theory and simulation are in agreement as long as the loop signal-to-noise ratio (SNR) is "high." For low loop SNR, the loop is nonlinear and the performance is degraded. Note from Fig. 6 that the noise power spectrum is not always white in the loop bandwidth, hence Eq. (20) can not be simplified any further in general.

III. Performance in a Dynamic Environment

The performance of the FEKF in a dynamic environment can only be assessed through simulations. In order to compare the performance with other schemes, the FEKF was tested in the presence of the identical dynamics described in [9], which exhibit two 100 g/sec jerks lasting for 0.5 sec each. For a fixed sampling time of 2 msec, the best performance in terms of lowest achievable CNR threshold is obtained when α is 1.005 and N_J is equal to 300. This corresponds to 22.5 dB-Hz (Fig. 7) with an rms frequency error 41.2 Hz (Fig. 8). The loop bandwidth at threshold is about 7.1 Hz with a 35.2 Hz steady-state error due to the jerk. The contribution of the noise in the linear model is about 27.3 Hz. Note that for fixed α and N_J, the loop bandwidth is a function of CNR as mentioned earlier.

Compared with other frequency tracking schemes using the same trajectory, the threshold of the FEKF is 3.5 dB lower than the PLL, 2.2 dB better than the CPAFC loop, 1.5 dB better than a fourth-order EKF tracking phase, and finally 0.5 dB more efficient than the approximate Maximum Likelihood (ML) scheme described in [9]. However in terms of rms frequency error, the FEKF is worse than all the above loops except for the CPAFC loop which exhibits an inferior performance. In terms of complexity, the FEKF requires the same number of computations per update as the PLL when implemented in the steady state.

IV. Conclusion

A new AFC loop was introduced and analyzed. The heart of the loop involves an EKF which operates on a modified set of data in order to track the frequency. The scheme can also be viewed as a modification of the well known cross-product AFC loop.

A detailed analysis of the second-order loop was presented and verified via simulations. The parameters of the FEKF were related to tracking parameters such as loop bandwidth and frequency jitter due to noise. The steady-state error due to jerk was also assessed.

The algorithm is best suited for scenarios in which frequency error is of secondary value and lowest operating CNR threshold is of primary concern. This technique is easily implemented and requires a minimum amount of computations per update. Moreover, it is highly suited for the ARX as it requires minimum software changes.

References

[1] B. D. O. Anderson and J. B. Moore, *Optimal Filtering*, New Jersey: Prentice Hall, 1979.

[2] D. R. Polk and S. C. Gupta, "Quasi-Optimum Digital Phase Locked Loops," *IEEE Trans. Comm.*, pp. 75–82, January 1973.

[3] F. R. Castella, "An Adaptive Two-Dimensional Kalman Tracking Filter," *IEEE Trans. Aero. Elec. Sys.*, vol. AES-16, no. 6, pp. 822–829, November 1973.

[4] B. Friedland, "Optimum Steady-State Positions and Velocity Estimation Using Noisy Sampled Position Data," *IEEE Trans. Aero. Elec. Sys.*, vol. 9, pp. 906–911, November 1973.

[5] W. C. Lindsey, *Synchronization Systems in Communication and Control*, New Jersey: Prentice Hall, 1972.

[6] F. D. Natali, "AFC Tracking Algorithms," *IEEE Trans. Comm.*, vol. COM-32, no. 8, pp. 935–947, August 1984.

[7] W. J. Hurd, J. I. Statman, and V. A. Vilnrotter, "High Dynamic GPS Receiver Using Maximum Likelihood Estimation and Frequency Tracking," *IEEE Trans. Aero. Elec. Sys.*, vol. AES-23, no. 4, pp. 925–937, July 1987.

[8] R. Kumar, "Differential Sampling for Fast Frequency Acquisition Via Adaptive Extended Least Squares Algorithm," *Proceedings of the International Telemetering Conference*, San Diego, California, pp. 191–201, October 1987.

[9] V. A. Vilnrotter, S. Hinedi, R. Kumar, *A Comparison of Frequency Estimation Techniques for High Dynamic Trajectories*, JPL Publication 88-21, Jet Propulsion Laboratory, Pasadena, California, September 15, 1988.

[10] B. Ekstrand, "Analytical Steady State Solution for a Kalman Tracking Filter," *IEEE Trans. Aero. Elec. Sys.*, vol. AES-19, no. 6, pp. 815–819, November 1983.

[11] E. I. Jury, *Theory and Application of the Z-Transform Method*, New York: Wiley, 1964.

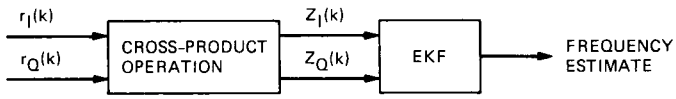

Fig. 1. General block diagram of the FEKF.

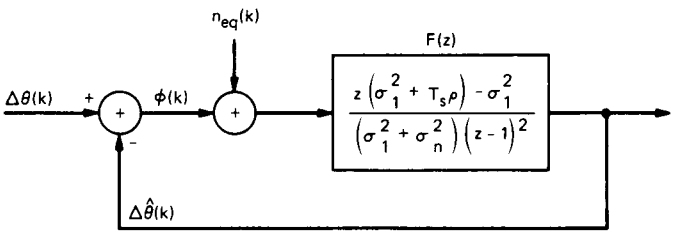

Fig. 2. Equivalent linear model of the second-order FEKF.

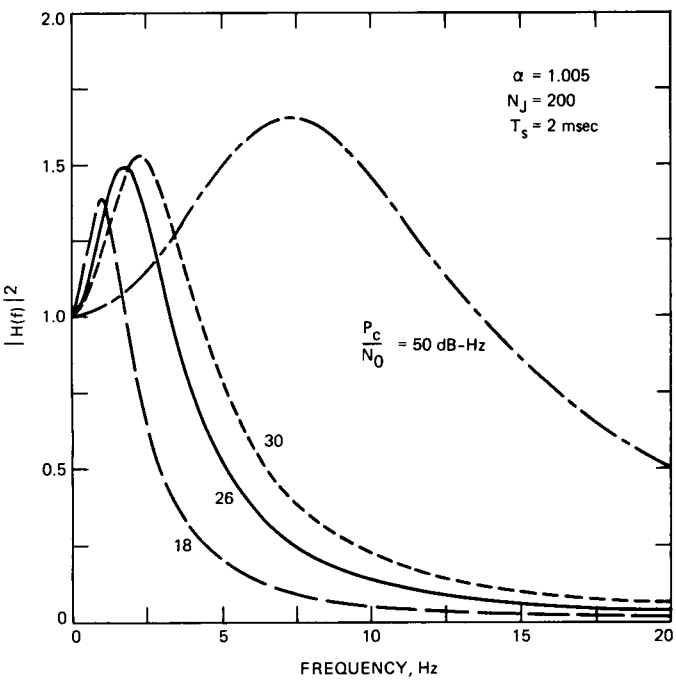

Fig. 3. Closed loop transfer function.

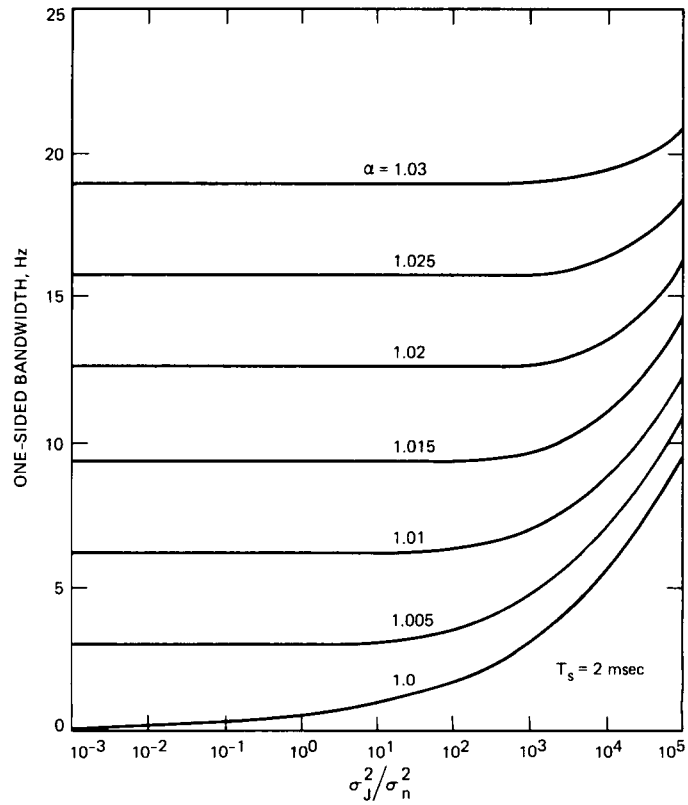

Fig. 4. Loop bandwidth.

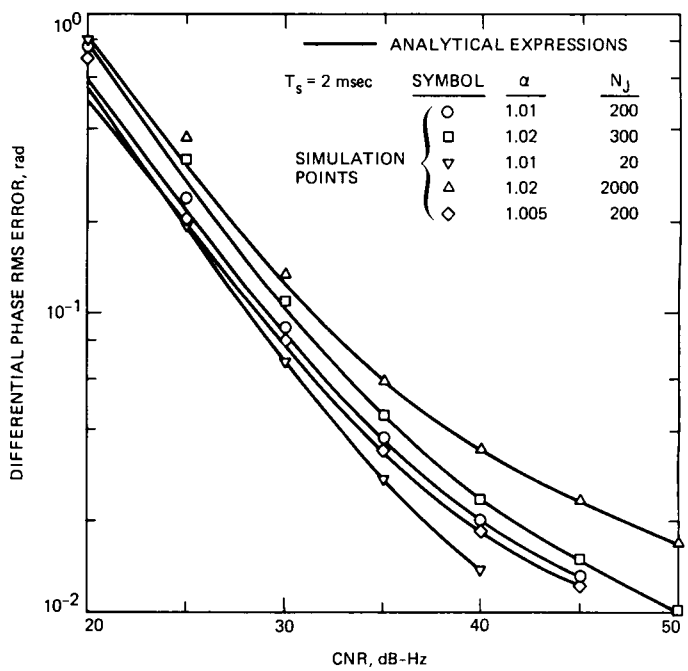

Fig. 5. Differential phase error versus CNR.

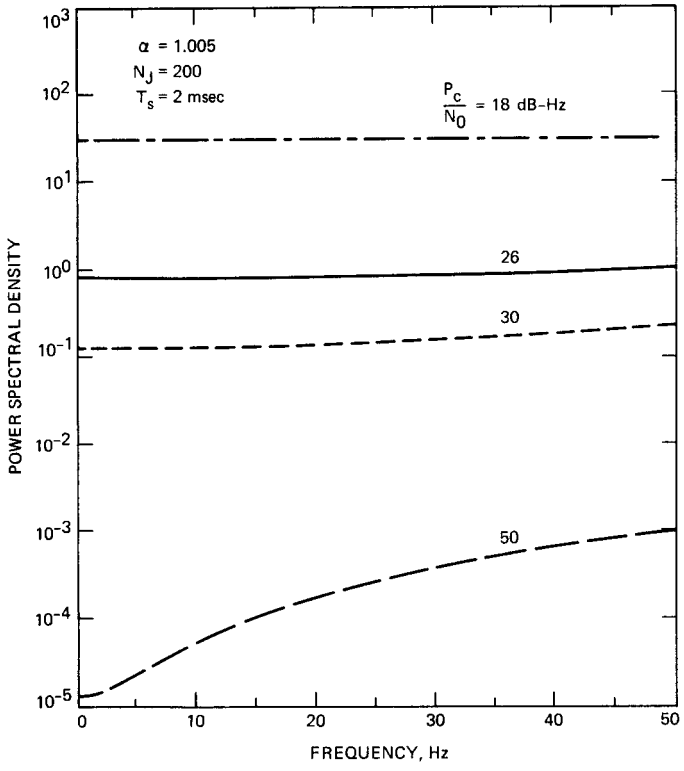

Fig. 6. Equivalent noise power spectral density.

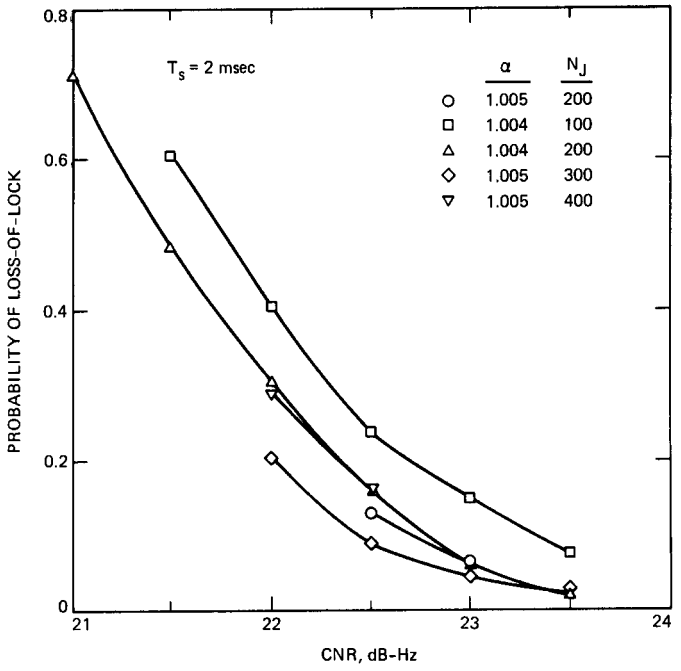

Fig. 7. Probability of loss-of-lock versus CNR.

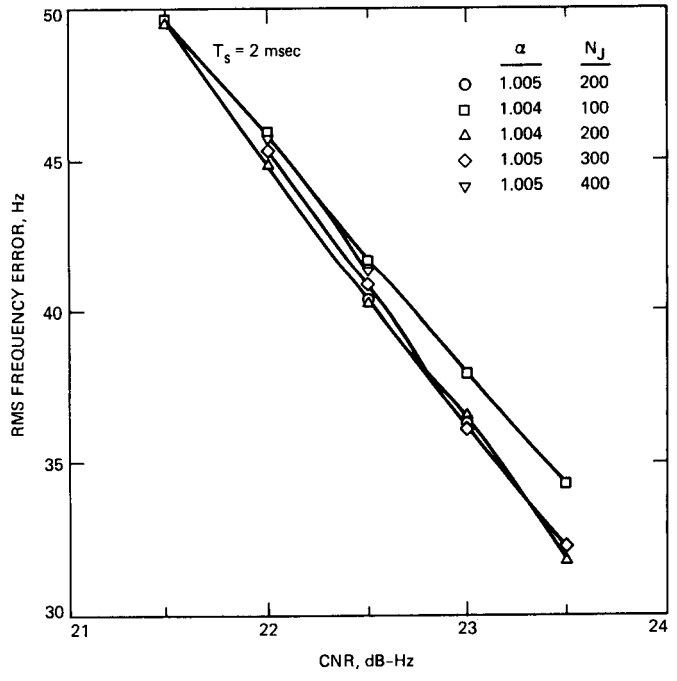

Fig. 8. RMS frequency error versus CNR.

Appendix
Performance of the FEKF in the Steady State

The error covariance matrix $\underline{\underline{\Sigma}}(k+1/k)$ satisfies the recursive Eq. (15c) which seems to depend on $\Delta\hat{\theta}(k/k-1)$. Defining the matrix

$$\underline{\underline{\Omega}}(k) = \underline{\underline{H}}^T(k)\,\underline{\underline{\Sigma}}(k/k-1)\,\underline{\underline{H}}(k) + \underline{\underline{R}} \tag{A-1}$$

and replacing $\underline{\underline{\Sigma}}(k/k-1)$ by its steady-state value given by Eq. (18), we have (letting $\underline{x}$ denote $\Delta\hat{\theta}(k/k-1)$)

$$\underline{\underline{\Omega}} = \begin{bmatrix} \cos x & 0 \\ -\sin x & 0 \end{bmatrix} \begin{bmatrix} \sigma_1^2 & \rho \\ \rho & \sigma_2^2 \end{bmatrix} \begin{bmatrix} \cos x & -\sin x \\ 0 & 0 \end{bmatrix} + \begin{bmatrix} \sigma_n^2 & 0 \\ 0 & \sigma_n^2 \end{bmatrix}$$

$$= \begin{bmatrix} \sigma_1^2 \cos^2 x + \sigma_n^2 & -\sigma_1^2 \cos x \sin x \\ -\sigma_1^2 \cos x \sin x & \sigma_1^2 \sin^2 x + \sigma_n^2 \end{bmatrix} \tag{A-2}$$

Inverting $\underline{\underline{\Omega}}(k)$, we obtain

$$\underline{\underline{\Omega}}^{-1}(k) = \frac{1}{\sigma_n^2\,\sigma_1^2 + \sigma_n^4} \begin{bmatrix} \sigma_1^2 \sin^2 x + \sigma_n^2 & \sigma_1^2 \sin x \cos x \\ \sigma_1^2 \cos x \sin x & \sigma_1^2 \cos^2 x + \sigma_n^2 \end{bmatrix} \tag{A-3}$$

which when pre- and post-multiplied by $\underline{\underline{H}}(k)$ gives

$$\underline{\underline{H}}(k)\,\underline{\underline{\Omega}}^{-1}(k)\,\underline{\underline{H}}^T(k) = \begin{bmatrix} \cos x & -\sin x \\ 0 & 0 \end{bmatrix} \cdot \underline{\underline{\Omega}}^{-1}(k) \begin{bmatrix} \cos x & 0 \\ -\sin x & 0 \end{bmatrix}$$

$$= \frac{1}{\sigma_1^2 + \sigma_n^2} \begin{bmatrix} 1 & 0 \\ 0 & 0 \end{bmatrix} \tag{A-4}$$

which is independent of $\Delta\hat{\theta}(k/k-1)$. The steady-state matrix $\overline{\Sigma}$ can be computed in closed form only when α is equal to one [10], otherwise the solution can only be obtained numerically. One approach is to run the FEKF until it reaches steady state and the resulting matrix is a solution of Eq. (15c) because of the properties of Kalman filters. Note also that the linear measurement (i.e., $z(k) = \Delta\theta(k) + n'(k)$) with $\underline{H}^T = [1 \;\; 0]$ would have resulted in the same matrix as in Eq. (A-4) and hence in the identical matrix $\overline{\Sigma}$.

In the steady state, the measurement vector $z(k)$ is subtracted from the prediction $\underline{h}(\cdot)$ before being multiplied by the gain matrix $\underline{\underline{K}}(k)$ as in Eq. (15a). Defining $\underline{\underline{L}}(k)$ to be

$$\underline{\underline{L}}(k) = \sum\!\!\!\!\!\!\sum (k/k-1)\,\underline{\underline{H}}(k)\,\underline{\underline{\Omega}}^{-1}(k) \tag{A-5}$$

we obtain in the steady state ($x \triangleq \Delta\hat{\theta}(k/k-1)$)

$$\underline{\underline{L}}(k) = \begin{bmatrix} \sigma_1^2 & \rho \\ \rho & \sigma_2^2 \end{bmatrix} \begin{bmatrix} \cos x & -\sin x \\ 0 & 0 \end{bmatrix} \underline{\underline{\Omega}}^{-1}(k)$$

$$= \frac{1}{\sigma_n^2 + \sigma_n^2} \begin{bmatrix} \sigma_1^2 \cos x & -\sigma_1^2 \sin x \\ \rho \cos x & -\rho \sin x \end{bmatrix} \tag{A-6}$$

which when multiplied by $\underline{z}(k) - \underline{h}(\cdot)$ yields

$$\underline{\underline{L}}(k)\,[\underline{z}(k) - h(\hat{\underline{x}}(k/k-1))] = \underline{\underline{L}}(k) \begin{bmatrix} z_I(k) - \sin\Delta\hat{\theta}(k/k-1) \\ z_Q(k) - \cos\Delta\hat{\theta}(k/k-1) \end{bmatrix}$$

$$= [z_I(k)\cos\Delta\hat{\theta}(k/k-1) - z_Q(k)\sin\Delta\hat{\theta}(k/k-1)] \cdot \frac{1}{\sigma_1^2 + \sigma_n^2} \begin{bmatrix} \sigma_1^2 \\ \rho \end{bmatrix} \tag{A-7}$$

Equation (A-7) combined with Eq. (15a) suggests the structure depicted in Fig. A-1. The output of the frequency disciminator $d(k)$ is given by

$$d(k) = z_I(k)\sin\Delta\hat{\theta}(k/k-1) - z_q(k)\cos\Delta\hat{\theta}(k/k-1) \tag{A-8}$$

Using Eq. (6), $d(k)$ simplifies to

$$d(k) = \sin\phi(k) + n_{eq}(k) \tag{A-9}$$

where $q(k)$ denotes the differential phase error and

$$n_{eq}(k) = n_I'(k)\cos\Delta\hat{\theta}(k/k-1) - n_q'(k)\sin\Delta\hat{\theta}(k/k-1) \tag{A-10}$$

It is straightforward to show that

$$\begin{aligned} E[n_{eq}^2(k)] &= 2(\sigma^2+\sigma^4) \\ E[n_{eq}(k)\,n_{eq}(k\pm1)] &= -\sigma^2\cos[\phi(k)-\phi(k-1)] \end{aligned} \tag{A-11}$$

which, assuming zero error, results in the following power spectrum

$$S_{n_{eq}}(z) = -\sigma^2 z + 2(\sigma^2+\sigma^4) - \sigma^2 z^{-1} \tag{A-12}$$

The resulting nonlinear model is shown in Fig. A-2. Using z-transforms, it is straightforward to show that

$$\underline{\hat{X}}(z) = \frac{1}{(z-1)^2}\begin{bmatrix} z-1 & T_s \\ 0 & z-1 \end{bmatrix}\underline{W}(z) \tag{A-13}$$

where $\underline{\hat{X}}(z)$ and $\underline{W}(z)$ are the $\underline{z}$-transforms of $\underline{\hat{x}}(k/k-1)$ and $\underline{\omega}(k)$, respectively. The loop filter $F(z)$ is then easily derived and is equal to

$$\begin{aligned} F(z) &= [1\ \ 0]\frac{1}{(z-1)^2}\begin{bmatrix} z-1 & T_s \\ 0 & z-1 \end{bmatrix}\begin{bmatrix} 1 & T_s \\ 0 & 1 \end{bmatrix} \\ &\quad\cdot\frac{1}{(\sigma_1^2+\sigma_n^2)}\begin{bmatrix}\sigma_1^2 \\ \rho\end{bmatrix} \\ &= \frac{z(\sigma_1^2+T_s)-\sigma_1^2}{(\sigma_1^2+\sigma_n^2)(z-1)^2} \end{aligned} \tag{A-14}$$

Figure A-3 depicts the simplified nonlinear model in terms of the loop filter $F(z)$. Approximating $\sin(\phi(k))$ by $\phi(k)$ for small error, we have, using operator notation

$$\phi(z) = [1-H(z)]\,\Delta\theta(z) - H(z)\{n_{eq}(k)\} \tag{A-15}$$

where $H(z)$ is the closed loop transfer function given by

$$H(z) = \frac{F(z)}{1+F(z)} = \frac{z(\sigma_1^2+T_s\rho)-\sigma_1^2}{z^2(\sigma_1^2+\sigma_n^2)+z(T_s\rho-\sigma_1^2-2\sigma_n^2)+\sigma_n^2} \tag{A-16}$$

From classical digital phase locked loop analysis, it is straightforward to show that the error in the absence of dynamics is given by

$$\sigma_\phi^2 = T_s\int_{\frac{-1}{2T_s}}^{\frac{1}{2T_s}}\left|H\left(e^{j2\pi fT_s}\right)\right|^2 S_{n_{eq}}\left(e^{j2\pi fT_s}\right)df \tag{A-17}$$

while the steady-state error due to jerk (in units of m/sec^3) is

$$\phi_{ss}(rad) = \left(\frac{\omega_i}{c}\right)\frac{J_0T_s^2}{\rho}(\sigma_1^2+\sigma_n^2) \tag{A-18}$$

where ω_i is the radian frequency of the incoming signal and c the velocity of light (in m/sec). The one-sided closed loop bandwidth $B_L(Hz)$ defined by

$$B_L(Hz) = \frac{1}{2T_s}\frac{1}{H^2(1)}\frac{1}{2\pi i}\oint H(z)\,H(z^{-1})\frac{dz}{z} \tag{A-19}$$

can be computed in closed form using the results found in [11] to give

$$B_L(Hz) = \frac{1}{2T_s}\frac{B_0e_1 - B_1a_1}{(a_0^2-a_2^2)(a_0+a_2)-(a_0-a_2)a_1^2}$$

where

$$\left.\begin{aligned} b_2 &= -\sigma_1^2;\ b_1 = \sigma_1^2+T_s\rho \\ a_2 &= \sigma_n^2;\ a_1 = T_s\rho-\sigma_1^2-2\sigma_n^2 \\ a_0 &= \sigma_1^2+\sigma_n^2 \end{aligned}\right\} \tag{A-20}$$

and

$$\left.\begin{aligned} B_0 &= b_1^2+b_2^2;\ B_1 = 2b_1b_2 \\ e_1 &= a_0+a_2 \end{aligned}\right\} \tag{A-21}$$

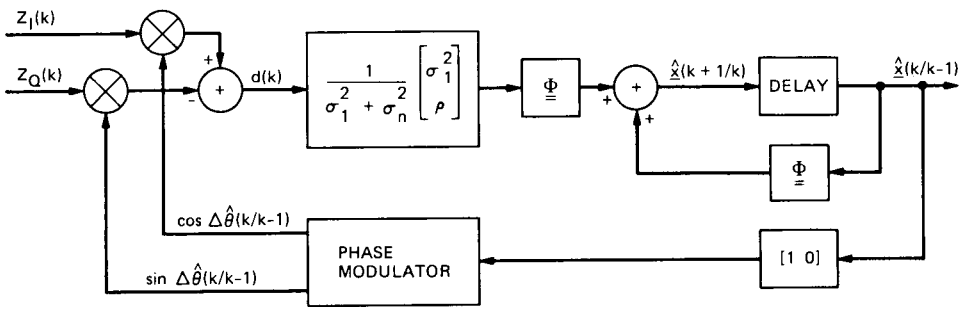

Fig. A-1. Equivalent steady-state model.

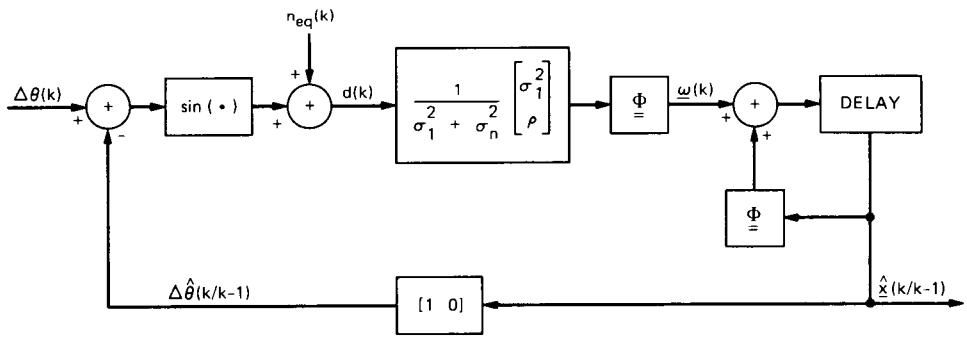

Fig. A-2. Equivalent nonlinear model.

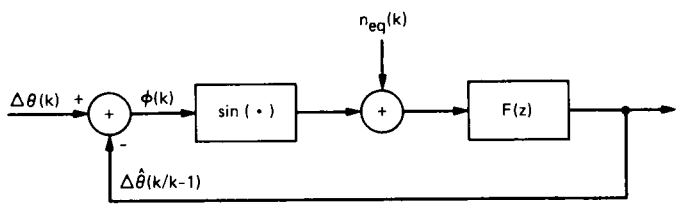

Fig. A-3. Simplified nonlinear model.